Volume 1 | Number 1 | Jan 2013 | Pages 1–100

Journal of
Materials Chemistry A

Materials for energy and sustainability
www.rsc.org/materialsA

Li⁺

ROYAL SOCIETY
OF CHEMISTRY

ROYAL SOCIETY
OF **CHEMISTRY**

www.rsc.org/materialsA

Journal of Materials Chemistry A

COMMUNICATION

Nanosized Pt anchored onto 3D nitrogen-doped graphene nanoribbons towards efficient methanol electrooxidation

Huajie Huang,‡[abd] Gonglan Ye,‡[a] Shubin Yang,[ae] Huilong Fei,[c] Chandra Sekhar Tiwary,[a] Yongji Gong,[c] Robert Vajtai,[a] James M. Tour,[ac] Xin Wang*[b] and Pulickel M. Ajayan*[ac]

The design and construction of nanostructured electrode catalysts with high activity at low cost are crucial elements in fuel cell technologies. Here, we demonstrate a combined hydrothermal self-assembly, freeze-drying, and thermal annealing approach for the fabrication of a hybrid catalyst made from nanosized Pt particles and three-dimensional (3D) nitrogen-doped graphene nanoribbons (N-GNRs). The resulting 3D architecture possesses large surface area, interconnected porous networks, uniform nitrogen distribution, extremely small sizes of Pt NPs and good electrical conductivity, which are highly desirable for electrocatalysis of methanol oxidation reaction. As a consequence, remarkable electrocatalytic properties including exceptional electrocatalytic activity, strong poison tolerance as well as superior long-term stability are achieved for Pt/N-GNR architecture, all of which are outperforming those observed for Pt/Vulcan XC-72 (Pt/C), Pt/carbon nanotube (Pt/CNT) and Pt/undoped GNR (Pt/GNR) catalysts.

Direct methanol fuel cells (DMFCs) have gained extensive attention as one of the important complements to secondary batteries due to their high operating power density and low pollutant emission properties.[1-3] Although platinum-based catalysts exhibit significant electrocatalytic activity for methanol oxidation in DMFCs, the expense of Pt catalysts and their poor tolerance to poisoning by by-products and impurities have hampered the scale-up of their use in applications.[4-7] One effective strategy to solve this problem is to develop Pt-carbon hybrids by homogeneously dispersing Pt nanoparticles (NPs) onto the surface of various carbons with high surface areas, such as carbon black,[8-10] carbon nanotubes,[11-14] porous carbon[15-19] and heteroatom-doped carbon.[20-24] In particular, nitrogen doping of carbon materials could affect their electronic structure and chemical reactivity, leading to smaller Pt NPs as well as strengthening the interaction of the carbon materials with the Pt.[25-27] In addition, the nitrogen component in the hybrid systems could provide surface hydroxyl species during the catalytic process, consequently accelerating the destruction of the absorbed intermediate carbonaceous species (mainly CO), thereby prolonging the catalytic activity of Pt.[28-30]

Very recently, graphene and graphene nanoribbons (GNRs), with properties including ultrahigh surface area, good flexibility and excellent chemical stability, have shown promise in DMFC applications.[31-36] Extensive theoretical and experimental investigations have demonstrated that the substituted N atoms are more likely to be distributed at the more reactive edge positions than in the inert basal planes.[37-39] Within this context, the presence of a high percentage of straight edges in narrow GNRs is conducive to acquiring doped carbon supports with a uniform N distribution, which is very difficult to achieve using 2D graphene sheets as well as other carbon materials.[40,41] The highly dispersed N atoms embedded in GNR frameworks would be expected to stabilize Pt NPs and eliminate residues that might poison the catalyst, thus significantly boosting the methanol oxidation efficiency. Moreover, the 1D GNRs could also serve as building blocks to construct 3D architectures, which would avoid the irreversible re-aggregation or re-stacking of alternate carbon materials such as graphene, that originates from strong van der Waals forces between the 2D sheets.[42,43] Therefore, the use of GNRs offers a good opportunity to develop novel Pt-decorated 3D carbon catalysts endowed with outstanding electrocatalytic properties.

In this work, we present the fabrication of Pt nanoparticles anchored on 3D N-doped GNRs (denoted as Pt/N-GNR) as anode electrocatalysts for methanol oxidation. The as-prepared 3D hybrid possesses large surface area, interconnected porous networks, and uniform nitrogen

[a.] Department of Materials Science and NanoEngineering, Rice University, Houston, Texas 77005, United States. E-mail: ajayan@rice.edu
[b.] Key Laboratory for Soft Chemistry and Functional Materials, Ministry of Education, Nanjing University of Science and Technology, Nanjing 210094, China. E-mail: wangx@mail.njust.edu.cn
[c.] Department of Chemistry, Rice University, Houston, Texas 77005, United States.
[d.] College of Mechanics and Materials, Hohai University, Nanjing 210098, China.
[e.] School of Materials Science and Engineering, Beihang University, Beijing 100191, China.
† Electronic Supplementary Information (ESI) available: Additional information and figures. See DOI: 10.1039/x0xx00000x
‡ H.H. and G.L. contributed equally to this work.

distribution as well as good electrical conductivity. These features not only allow a rapid rate of diffusion of methanol electrolyte, but also provide numerous electroactive sites. As a consequence, the 3D Pt/N-GNR architecture has high forward anodic peak current density and exceptional poison tolerance with superior long-term stability, outperforming commercial Pt/Vulcan XC-72 (Pt/C), Pt/carbon nanotube (Pt/CNT) and Pt/undoped GNR (Pt/GNR) hybrids when they are employed as methanol oxidation catalysts.

The overall synthetic procedure to 3D Pt/N-GNR architecture is illustrated in Fig. 1a. First, 1D GONR strips (Fig. S1) were produced by unzipping MWCNTs through a solution-based oxidative route.[44,45] Then the as-prepared GONR dispersion was transferred into a Teflon-autoclave and maintained at a constant temperature of 180 °C for 12 h. During this hydrothermal process, the GONRs, with abundant oxygen-containing functional groups, act as building blocks to construct 3D interpenetrating hydrogels. After freezing drying using a high vacuum pump, the resulting samples were annealed under a NH_3 atmosphere at 900 °C for 0.5 h, a reaction during which the incorporation of N atoms into the carbon framework and the deoxygenation of GONRs occurred. In the final reaction step, Pt NPs were slowly nucleated on the surfaces of the as-prepared 3D monolithic N-GNRs in ethylene glycol, giving birth to the Pt/N-GNR architecture.
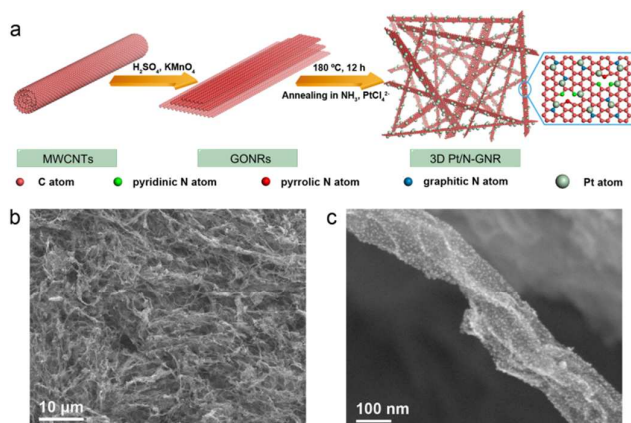

Fig. 1 (a) Schematic of the fabrication process for the 3D Pt/N-GNR architecture. It includes three steps: (1) preparation of GNRs through solution-based chemical unzipping of MWCNTs; (2) construction of 3D porous GNR architectures *via* hydrothermal reaction and the incorporation of N atoms into the GNR skeletons by heating treatment under NH_3; (3) controllable deposition of Pt NPs on the surfaces of the N-GNRs. Typical (b) low- and (c) high-magnification FE-SEM images of the Pt/N-GNR composite, revealing a 3D porous interconnected N-GNR architecture with numerous Pt NPs.

The microstructural features of as-prepared Pt/N-GNR were initially observed by means of field-emission scanning electron microscopy (FE-SEM) and transmission electron microscopy (TEM). As depicted in Fig. 1b and S2a, typical SEM images of Pt/N-GNR reveal a highly interpenetrating and porous 3D network, which is composed of numerous thin and flexible ribbons without obvious collapsing or cracking. The typical sizes of these N-containing nanoribbons range from tens to

hundreds of nm in width and several tens of μm in length. The GNR building blocks were decorated by Pt NPs with a narrow particle size distribution (Fig. 1c, 2a and 2b). Such a good dispersion is attributed to the interconnected porous structure as well as the large presence of N atoms in the materials, which could provide multiple accessible platforms for the deposition of Pt NPs and simultaneously enhance the interaction between the metal and carbon supports.[27,46,47] Moreover, distinguishable lattice fringes for face-centered cubic (fcc) Pt crystals and GNRs are clearly observed in the electronic diffraction patterns and high-resolution TEM (HRTEM) images of the Pt/N-GNR (the insets of Fig. 2a, c and Fig. 2c-f), and the corresponding crystal plane distances are in good agreement with the known data.[48,49] Further inspection by the elemental mappings disclose that the Pt/N-GNR architecture contains C, N and Pt as the main components, and the elements are homogeneously distributed over the entire areas of the ribbons (Fig. 2g-j). It is worth mentioning here that since the Pt-N_5 ionization energy is below the C-K and N-K energy filter, the disturbances from Pt signals in carbon and nitrogen mappings are inevitable.[29,50] For comparison, Pt/GNR, Pt/CNT and Pt/C composites were also synthesized using procedures similar to those for Pt/N-GNR but the N-GNRs were replaced by the other carbon supports. As shown in Fig. S2b-d and S3, the Pt NPs were prone to aggregate and form large clusters in these samples, probably as a result of the lack of effective anchor sites and relatively small surface areas.[20,51,52]
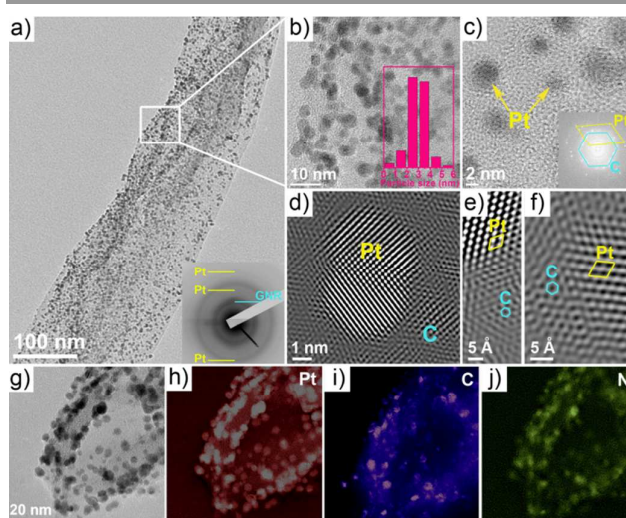

Fig. 2 TEM analysis of the Pt/N-GNR architecture. Representative (a and b) TEM images and (c-f) HRTEM images of Pt/N-GNR demonstrate the efficient loading of crystalline Pt NPs with an average diameter of 3.1 nm on ultrathin N-GNRs. Insets in (a-c): the selected area electronic diffraction (SAED) pattern, Pt NP size distribution and fast Fourier transform (FFT)-generated SAED pattern of Pt/N-GNR, respectively. (g) Scanning transmission electron microscopy (STEM) image and corresponding elemental mapping of (h) Pt, (i) C, and (j) N elements, showing the homogeneous dispersion of Pt, C and N in the ribbons.

To gain additional insight into the elemental composition and chemical states of the Pt/N-GNR architecture, X-ray photoelectron spectroscopy (XPS) measurements and elemental analysis were done. As presented in Fig. 3a, the

survey scan spectrum of Pt/N-GNR discloses the coexistence of C, N and Pt components without detecting any impurities. Remarkably, owing to the abundant edge structure, the nitrogen content of Pt/N-GNR was as high as 6.5 at%, which exceeds most reported nitrogen contents for N-doped graphene materials (< 5.0 at%).[40] The high resolution N1s spectrum (Fig. 3b) was resolved into three components at binding energies of 398.3, 399.5 and 401.2 eV, belonging to pyridinic N (N1), pyrrolic N (N2) and graphitic N (N3).[53,54] The first two N functionalities are reported to improve the growth behavior of metal particles, thus the high percentage of N1 and N2 atoms (~70.0% total) within the ribbon frameworks would significantly suppress the aggregation of Pt NPs and lead to a uniform dispersion of active sites.[55,56] In addition, as shown in Fig. 3c, the deconvolution of the complex C1s spectrum suggested four forms of carbon, sp^2 C-C (284.7 eV), sp^2 C-N (285.4 eV), C-OH (286.4 eV) and sp^3 C-N (287.1 eV).[57,58] Note that the intensities of the oxygenated functional groups in Pt/N-GNR are much weaker than those of pristine GONRs (Fig. S4), evidence of a high degree of reduction through the heat treatment process. Furthermore, two pairs of doublets were discerned in the high-resolution Pt 4f scans (Fig. 3d): the lower energy peaks (71.4 and 74.7 eV) were assigned to zero-valent metallic Pt, while the higher energy peaks (72.0 and 76.0 eV) were due to the 2+ oxidation state of Pt.[59,60] These conclusions were also verified by X-ray diffraction (XRD), energy-dispersive X-ray (EDX) spectrum, and Raman analyses, demonstrating that the Pt NPs were successfully attached to the N-GNRs (Fig. S5-S7, respectively). In addition, N_2 adsorption–desorption isotherms given in Fig. S8 further validated the meso- and macroporous nature of the Pt/N-GNR architecture. Brunauer–Emmett–Teller (BET) analysis indicated that the specific surface area of Pt/N-GNR was as high as 341.0 m^2 g^{-1}, similar to those of recent state-of-the-art graphene aerogel-based nanostructures.[61-63]

To make use of their distinctive structural features, Pt/N-GNR were coated onto glassy carbon electrodes and subjected to cyclic voltammetry (CV) tests to assess their electrocatalytic activity. As seen from Fig. 4a and Fig. S9, all CV curves, recorded in N_2-purged 1 M H_2SO_4, showed obvious peaks in the potential region of -0.2 to 0.1 V, which are basically associated with the hydrogen adsorption processes. The integrated peak areas can be used to estimate the electrochemically active surface areas (ECSAs) for these four catalysts.[64,65] Based on the Pt mass, the specific ECSA of the as-obtained Pt/N-GNR was 64.6 m^2 g^{-1}, much higher than that obtained for Pt/GNR (39.8 m^2 g^{-1}), Pt/CNT (27.9 m^2 g^{-1}) or Pt/C (22.0 m^2 g^{-1}) samples (Fig. 4c). This result indicates that Pt/N-GNR is easily accessible for electrocatalytic reactions, hence providing a large amount of available catalytic sites. To evaluate the properties of various electrocatalysts toward methanol oxidation reactions, the CV measurements were also carried out in a solution containing 1 M H_2SO_4 and 2 M methanol. Strikingly, a very high forward anodic peak current density of 11.0 mA cm^{-2} was achieved for the reaction on the Pt/N-GNR electrode, which was 1.3, 1.7 or 2.5 times that of the Pt/GNR (8.6 mA cm^{-2}), Pt/CNT (6.5 mA cm^{-2}) or Pt/C (4.4 mA cm^{-2}) electrodes, respectively, consistent with the ECSA trend (Fig. 4b and d). Additionally, at a fixed oxidation current density (as indicated by the dashed line in Fig. S10), the corresponding potential of Pt/N-GNR was apparently lower than those of the reference samples, suggesting that the catalytic reaction was more facile on the Pt/N-GNR electrode surface. On the other hand, the ratio of the forward-scan peak current (I_F) *versus* the reverse-scan peak current (I_R), I_F/I_R, is reported to be a critical indicator in describing the catalyst's tolerance toward the intermediate carbonaceous species (mainly CO).[59,66] As shown in Fig. 4d and Table 1, when compared with the Pt/GNR, Pt/CNT or Pt/C catalysts, Pt/N-GNR exhibited 23%, 18% or 37% enhancement in I_F/I_R, respectively, most likely a result of its high nitrogen content, which could polarize adjacent carbon atoms and assist the water dissociation reaction to generate hydroxyl sources for oxidation of carbonaceous residues.[28,30]
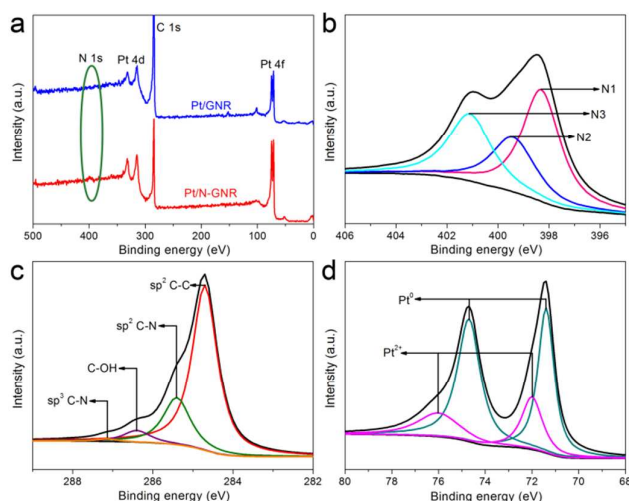

Fig. 3 XPS spectra of the Pt/N-GNR architecture. (a) The XPS survey spectra indicate that Pt/N-GNR has a high nitrogen content. High-resolution (b) N 1s, (c) C 1s, and (d) Pt 4f XPS spectra of Pt/N-GNR, implying that N-GNRs and metallic Pt coexist in the Pt/N-GNR architecture.
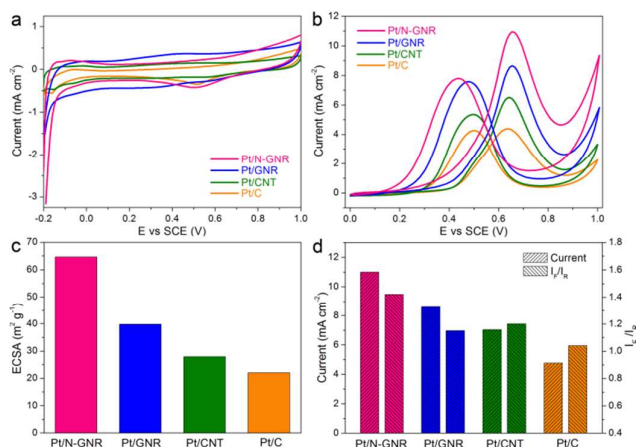

Fig. 4 Electrocatalytic activity of the Pt/N-GNR architecture in the electrooxidation of methanol. Cyclic voltammograms of Pt/GNR, Pt/N-GNR,

COMMUNICATION

Pt/CNT and Pt/C catalysts in (a) 1 M H_2SO_4 solution and (b) 1 M H_2SO_4 with 2 M methanol solution at a scan rate of 20 mV s^{-1}. (c) Specific ECSAs and (d) forward anodic peak current densities as well as I_F/I_R ratios for these four catalysts, establishing the largest ECSA value and the highest catalytic activity of Pt/N-GNR.

Table 1 Compiled study comparing CV results for different catalysts.

Electrode	ECSA (m^2 g^{-1})	I_F (mA cm^{-2})	I_R (mA cm^{-2})	I_F/I_R Ratio
Pt/N-GNR	64.6	11.0	7.7	1.42
Pt/GNR	39.8	8.6	7.5	1.15
Pt/CNT	27.9	6.5	5.4	1.20
Pt/C	22.0	4.4	4.2	1.04

The long-term durability of electrocatalysts is a crucial requirement for their practical usage in fuel cell systems. The chronoamperometric technique was employed to compare the electrocatalytic stability of different catalysts. As seen in Fig. 5a, when a constant potential was applied, the current density of all electrodes decreased with time, arising from the gradual accumulation of poisoning species on the catalytic sites as well as the unavoidable formation of Pt-oxides.[35,67,68] It was found that the Pt/N-GNR catalyst only lost ~38.1% of its initial current density after 2000 s, which is more competitive than Pt/GNR (~72.7% loss after 2000 s), Pt/CNT (~81.6% loss after 2000 s), Pt/C (~79.1% loss after 2000 s) and those of recent state-of-the-art Pt-based nanostructures such as Pt/ionic liquid/CNT,[69] Pt/polyaniline,[70] Pt/graphene,[59,60,71] Pt-on-Pd nanodendrites,[72] spherical Pt-Zn nanocrystals,[73] Pt/C$_3$N$_4$/graphene,[29] Pt-Ni$_2$P/C,[10] etc., proving that our Pt/N-GNR catalyst has outstanding catalytic stability for methanol oxidation. TEM analysis revealed that the Pt/N-GNR architecture, after being subjected to the durability test, displayed negligible deterioration in its structural integrity, where a minority of the GNRs were re-stacked and the well-dispersed Pt NPs maintained their crystalline (111) plane structure (Fig. S11a and b). However, as for the contrasting samples, the Pt NPs became distinctly larger and readily formed aggregates, as emphasized by the circled agglomerates in Fig. S11c-h. In addition, chronopotentiometric measurements were conducted over the potential range from 0 to 1 V to further demonstrate the excellent anti-poisoning ability of N-GNRs supported catalysts. After applying a fixed anodic current, the intermediate carbonaceous species are accumulated on the electrode surface and lower the catalytic activity of the electrocatalysts. In order to satisfy the applied current, the potential must increase to a higher level at which larger amounts of H_2O can be decomposed.[74] It is seen from Fig. 5b that the electrode potentials of all catalysts rose steadily for a period of time and then abruptly jumped to a much higher value. The time before the potential jumps is able to reflect the catalyst's tolerance to the carbonaceous residues accumulation.[75] Among these four catalysts, Pt/N-GNR not only had the lowest onset potential, but also sustained the longest time, indicating that the novel structural design of 3D nitrogen-enriched Pt/N-GNR is very beneficial to the elimination of the poisoning species during the catalytic process.

It is worth mention that the remarkably enhanced electrocatalytic performance of Pt/N-GNR originates from multiple synergistic effects within its sophisticated construction, which can be summarized as follows. First, the interconnected 3D porous framework provides extremely high surface areas that host sufficient active sites and facilitate the transportation of the external electrolyte into the interior surfaces. Second, the existence of large quantities of N atoms substantially reinforces the interfacial contact between the Pt NPs and the N-GNRs, and at the same time keeps the Pt sites clean through high-efficiency oxidative removal of the absorbed carbonaceous intermediates. Third, the N-GNR backbone acts as a high-speed electronic conductive channel, enabling a high electron transfer number and a large population of the triple-phase boundaries on electrode surface.[76,77] As presented in Fig. 5c, d and Fig. S12, electrochemical impedance spectroscopy (EIS) results reveal that the Pt/N-GNR electrode maintains a low charge-transfer resistance of 3.9 Ω, more competitive than that of Pt/C (680.4 Ω) and close to those of Pt/GNR (2.7 Ω) and Pt/CNT (2.4 Ω) electrodes. Finally, the well-confined Pt NPs, with a homogeneous distribution in the 3D hybrid system, are able to exert their unique catalytic function and thus achieve an optimal Pt utilization. As a result of integrating these advantages, the Pt/N-GNR architecture holds great potential for use in advanced energy conversion devices.
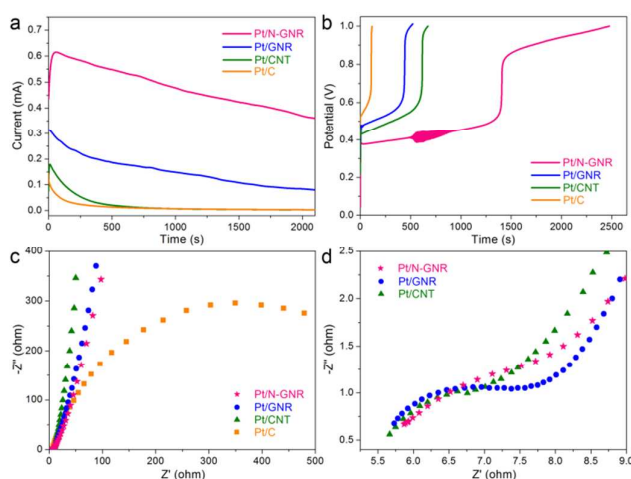

Fig. 5 Comparison of the electrocatalytic performance of the Pt/N-GNR, Pt/GNR, Pt/CNT and Pt/C catalysts. (a) Chronoamperometric responses recorded at 0.5 V (vs SCE (saturated calomel electrode)) and (b) chronopotentiometric curves of Pt/N-GNR, Pt/GNR, Pt/CNT and Pt/C in 1 M H_2SO_4 with 2 M methanol solution, confirming that Pt/N-GNR possesses the best long-term catalytic stability and the strongest anti-poisoning capacity among them. (c) Nyquist plots of Pt/N-GNR, Pt/GNR, Pt/CNT and Pt/C hybrids in 1 M H_2SO_4 with 2 M methanol solution at open circuit potential (vs. SCE). (d) Local enlargement of the Nyquist plots for Pt/GNR and Pt/N-GNR. The smaller circle diameter discloses that the charge-transfer resistance of the Pt/N-GNR electrode is significantly lower than that of control Pt/C electrode.

In summary, a new hybrid architecture consisting of Pt NPs grown on 3D porous N-GNRs has been successfully fabricated by a combined hydrothermal self-assembly, freeze-drying, and

thermal annealing process. The resulting Pt/N-GNR provides a series of favorable structural features, such as a 3D cross-linked porous network, large surface area, uniform nitrogen distribution, extremely small sizes of Pt NPs and good electrical conductivity, giving it exceptional electrocatalytic activity, strong poison tolerance as well as superior long-term stability toward electrochemical oxidation of methanol. This work will pave the way to develop 3D heteroatom-doped GNRs supported nanomaterials for a variety of applications including supercapacitors, lithium batteries, photocatalysis, and sensors.

Acknowledgements

Notes and references

1   B. C. H. Steele and A. Heinzel, *Nature*, 2001, **414**, 345.
2   N. Kakati, J. Maiti, S. H. Lee, S. H. Jee, B. Viswanathan and Y. S. Yoon, *Chem. Rev.*, 2014, **114**, 12397.
3   J. N. Tiwari, R. N. Tiwari, G. Singh and K. S. Kim, *Nano Energy*, 2013, **2**, 553.
4   A. S. Aricò, P. Bruce, B. Scrosati, J.-M. Tarascon and W. Van Schalkwijk, *Nat. Mater.*, 2005, **4**, 366.
5   Y.-G. Guo, J.-S. Hu and L.-J. Wan, *Adv. Mater.*, 2008, **20**, 2878.
6   A. Chen and P. Holt-Hindle, *Chem. Rev*, 2010, **110**, 3767.
7   N. V. Long, Y. Yang, C. Minh Thi, N. V. Minh, Y. Cao and M. Nogami, *Nano Energy*, 2013, **2**, 636.
8   Y.-Y. Chu, Z.-B. Wang, Z.-Z. Jiang, D.-M. Gu and G.-P. Yin, *Adv. Mater.*, 2011, **23**, 3100.
9   S. K. Meher and G. R. Rao, *ACS Catal.*, 2012, **2**, 2795.
10 J. Chang, L. Feng, C. Liu, W. Xing and X. Hu, *Energy Environ. Sci.*, 2014, **7**, 1628.
11 L. Cao, F. Scheiba, C. Roth, F. Schweiger, C. Cremers, U. Stimming, H. Fuess, L. Chen, W. Zhu and X. Qiu, *Angew. Chem. Inter. Ed.*, 2006, **45**, 5315.
12 S. J. Liao, K. A. Holmes, H. Tsaprailis and V. I. Birss, *J. Am. Chem. Soc.*, 2006, **128**, 3504.
13 B. Wu, D. Hu, Y. Kuang, B. Liu, X. Zhang and J. Chen, *Angew. Chem. Inter. Ed.*, 2009, **48**, 4751.
14 S. J. Guo, S. J. Dong and E. K. Wang, *Adv. Mater.*, 2010, **22**, 1269.
15 G. Cui, L. Zhi, A. Thomas, U. Kolb, I. Lieberwirth and K. Müllen, *Angew. Chem. Inter. Ed.*, 2007, **46**, 3464.
16 G. S. Chai, I. S. Shin and J. S. Yu, *Adv. Mater.*, 2004, **16**, 2057.
17 F. Su, J. Zeng, X. Bao, Y. Yu, J. Y. Lee and X. S. Zhao, *Chem. Mater.*, 2005, **17**, 3960.
18 Z. Wen, J. Liu and J. Li, *Adv. Mater.*, 2008, **20**, 743.
19 H. Jiang, T. Zhao, C. Li and J. Ma, *Chem. Commun.*, 2011, **47**, 8590.
20 R. Lv, T. Cui, M.-S. Jun, Q. Zhang, A. Cao, D. S. Su, Z. Zhang, S.-H. Yoon, J. Miyawaki, I. Mochida and F. Kang, *Adv. Funct. Mater.*, 2011, **21**, 999.
21 V. Di Noto, E. Negro, R. Gliubizzi, S. Lavina, G. Pace, S. Gross and C. Maccato, *Adv. Funct. Mater.*, 2007, **17**, 3626.
22 C.-H. Hsu, H.-M. Wu and P.-L. Kuo, *Chem. Commun.*, 2010, **46**, 7628.
23 R. Ahmadi, M. K. Amini and J. C. Bennett, *J. Catal.*, 2012, **292**, 81.
24 B. Xiong, Y. Zhou, Y. Zhao, J. Wang, X. Chen, R. O'Hayre and Z. Shao, *Carbon*, 2013, **52**, 181.
25 S. Pylypenko, A. Borisevich, K. L. More, A. R. Corpuz, T. Holme, A. A. Dameron, T. S. Olson, H. N. Dinh, T. Gennett and R. O'Hayre, *Energy Environ. Sci.*, 2013, **6**, 2957.
26 T. Holme, Y. Zhou, R. Pasquarelli and R. O'Hayre, *Phys. Chem. Chem. Phys.*, 2010, **12**, 9461.
27 Y.-H. Li, T.-H. Hung and C.-W. Chen, *Carbon*, 2009, **47**, 850.
28 Y. Zhou, K. Neyerlin, T. S. Olson, S. Pylypenko, J. Bult, H. N. Dinh, T. Gennett, Z. Shao and R. O'Hayre, *Energy Environ. Sci.*, 2010, **3**, 1437.
29 H. Huang, S. Yang, R. Vajtai, X. Wang and P. M. Ajayan, *Adv. Mater.*, 2014, **26**, 5160.
30 G. Yang, Y. Li, R. K. Rana and J.-J. Zhu, *J. Mater. Chem. A*, 2013, **1**, 1754.
31 B. Xia, Y. Yan, X. Wang and X. W. Lou, *Mater. Horiz.*, 2014, **1**, 379.
32 X. Li, X. Wang, L. Zhang, S. Lee and H. Dai, *Science*, 2008, **319**, 1229.
33 A. L. Elías, A. s. R. Botello-Méndez, D. Meneses-Rodríguez, V. Jehová González, D. Ramírez-González, L. Ci, E. Muñoz-Sandoval, P. M. Ajayan, H. Terrones and M. Terrones, *Nano Lett.*, 2009, **10**, 366.
34 S. Guo, S. Dong and E. Wang, *Acs Nano*, 2010, **4**, 547.
35 Y. M. Li, L. H. Tang and J. H. Li, *Electrochem. Commun.*, 2009, **11**, 846.
36 M. Liu, R. Zhang and W. Chen, *Chem. Rev.*, 2014, **114**, 5117.
37 X. Wang, X. Li, L. Zhang, Y. Yoon, P. K. Weber, H. Wang, J. Guo and H. Dai, *Science*, 2009, **324**, 768.
38 M. Terrones, O. Martín, M. González, J. Pozuelo, B. Serrano, J. C. Cabanelas, S. M. Vega-Díaz and J. Baselga, *Adv. Mater.*, 2011, **23**, 5302.
39 Y. Li, Z. Zhou, P. Shen and Z. Chen, *Acs Nano*, 2009, **3**, 1952.
40 H. Wang, T. Maiyalagan and X. Wang, *ACS Catal.*, 2012, **2**, 781.
41 R. Cruz-Silva, A. Morelos-Gómez, S. Vega-Díaz, F. Tristán-López, A. L. Elias, N. Perea-López, H. Muramatsu, T. Hayashi, K. Fujisawa and Y. A. Kim, *Acs Nano*, 2013, **7**, 2192.
42 D. Li, M. B. Mueller, S. Gilje, R. B. Kaner and G. G. Wallace, *Nat. Nanotechnol.*, 2008, **3**, 101.
43 Y. Gong, S. Yang, L. Zhan, L. Ma, R. Vajtai and P. M. Ajayan, *Adv. Funct. Mater.*, 2014, **24**, 125.
44 D. V. Kosynkin, A. L. Higginbotham, A. Sinitskii, J. R. Lomeda, A. Dimiev, B. K. Price and J. M. Tour, *Nature*, 2009, **458**, 872.
45 A. L. Higginbotham, D. V. Kosynkin, A. Sinitskii, Z. Sun and J. M. Tour, *Acs Nano*, 2010, **4**, 2059.
46 Z. Tang, S. Shen, J. Zhuang and X. Wang, *Angew. Chem. Inter. Ed.*, 2010, **49**, 4603.
47 S. Zhao, H. Yin, L. Du, G. Yin, Z. Tang and S. Liu, *J. Mater. Chem. A*, 2014, **2**, 3719.
48 X. Huang, Z. Zeng, S. Bao, M. Wang, X. Qi, Z. Fan and H. Zhang, *Nat. Commun.*, 2013, **4**, 1444.
49 L. Ci, L. Song, C. Jin, D. Jariwala, D. Wu, Y. Li, A. Srivastava, Z. F. Wang, K. Storr, L. Balicas, F. Liu and P. M. Ajayan, *Nat. Mater.*, 2010, **9**, 430.
50 K. Ghosh, M. Kumar, H. Wang, T. Maruyama and Y. Ando, *J. Phys. Chem. C*, 2010, **114**, 5107.
51 D. He, Y. Jiang, H. Lv, M. Pan and S. Mu, *Appl. Cataly. B*, 2013, **132**, 379.
52 H. Huang, Q. Chen, M. He, X. Sun and X. Wang, *J. Power Sources*, 2013, **239**, 189.

53 X. Li, H. Wang, J. T. Robinson, H. Sanchez, G. Diankov and H. Dai, *J. Am. Chem. Soc.*, 2009, **131**, 15939.

54 Z.-H. Sheng, L. Shao, J.-J. Chen, W.-J. Bao, F.-B. Wang and X.-H. Xia, *Acs Nano*, 2011, **5**, 4350.

55 P.-L. Kuo and C.-H. Hsu, *Acs Appl. Mater. Interfaces*, 2010, **3**, 115.

56 C. Pan, L. Qiu, Y. Peng and F. Yan, *J. Mater. Chem.*, 2012, **22**, 13578.

57 D. Wei, Y. Liu, Y. Wang, H. Zhang, L. Huang and G. Yu, *Nano Lett.*, 2009, **9**, 1752.

58 A. L. M. Reddy, A. Srivastava, S. R. Gowda, H. Gullapalli, M. Dubey and P. M. Ajayan, *Acs Nano*, 2010, **4**, 6337.

59 S. Sharma, A. Ganguly, P. Papakonstantinou, X. P. Miao, M. X. Li, J. L. Hutchison, M. Delichatsios and S. Ukleja, *J. Phys. Chem. C*, 2010, **114**, 19459.

60 H. Huang, H. Chen, D. Sun and X. Wang, *J. Power Sources*, 2012, **204**, 46.

61 Z.-S. Wu, Y. Sun, Y.-Z. Tan, S. Yang, X. Feng and K. Müllen, *J. Am. Chem. Soc.*, 2012, **134**, 19532.

62 Z.-S. Wu, A. Winter, L. Chen, Y. Sun, A. Turchanin, X. Feng and K. Müllen, *Adv. Mater.*, 2012, **24**, 5130.

63 Y. Gong, S. Yang, Z. Liu, L. Ma, R. Vajtai and P. M. Ajayan, *Adv. Mater.*, 2013, **25**, 3979.

64 B. Lim, M. Jiang, P. H. C. Camargo, E. C. Cho, J. Tao, X. Lu, Y. Zhu and Y. Xia, *Science*, 2009, **324**, 1302.

65 A. Pozio, M. De Francesco, A. Cemmi, F. Cardellini and L. Giorgi, *J. Power Sources*, 2002, **105**, 13.

66 X. Cao, N. Wang, Y. Han, C. Gao, Y. Xu, M. Li and Y. Shao, *Nano Energy*, 2015, **12**, 105.

67 C. Wang, R. Yue, H. Wang, C. Zou, J. Du, F. Jiang, Y. Du, P. Yang and C. Wang, *Inter. J. Hydrogen Energy*, 2014, **39**, 5764.

68 C. Wang, F. Jiang, R. Yue, H. Wang and Y. Du, *J. Solid State Electrochem.*, 2014, **18**, 515.

69 H. Chu, Y. Shen, L. Lin, X. Qin, G. Feng, Z. Lin, J. Wang, H. Liu and Y. Li, *Adv. Funct. Mater.*, 2010, **20**, 3747.

70 S. Guo, S. Dong and E. Wang, *Small*, 2009, **5**, 1869.

71 Y. C. Xin, J. G. Liu, Y. Zhou, W. M. Liu, J. A. Gao, Y. Xie, Y. Yin and Z. G. Zou, *J. Power Sources*, 2011, **196**, 1012.

72 L. Wang, Y. Nemoto and Y. Yamauchi, *J. Am. Chem. Soc.*, 2011, **133**, 9674.

73 Y. Kang, J. B. Pyo, X. Ye, T. R. Gordon and C. B. Murray, *Acs Nano*, 2012, **6**, 5642.

74 M. Krausa and W. Vielstich, *J. Electroanal. Chem.*, 1995, **399**, 7.

75 J. H. Chen, M. Y. Wang, B. Liu, Z. Fan, K. Z. Cui and Y. Kuang, *J. Phys. Chem. B*, 2006, **110**, 11775.

76 C. A. Bessel, K. Laubernds, N. M. Rodriguez and R. T. K. Baker, *J. Phys. Chem. B*, 2001, **105**, 1115.

77 P. Kim, H. S. Kim, J. B. Joo, W. Y. Kim, I. K. Song and J. H. Yi, *J. Power Sources*, 2005, **145**, 139.

Graphical abstract
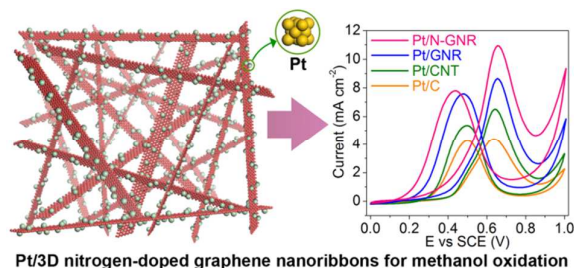
Pt/3D nitrogen-doped graphene nanoribbons for methanol oxidation

A combined hydrothermal self-assembly, freeze-drying, and thermal annealing approach is developed to homogeneously disperse nanosized Pt particles onto nitrogen-doped graphene nanoribbons (N-GNRs). Because of the attractive structural features, such as 3D cross-linked porous network, large surface area, uniform nitrogen distribution, extremely small particle size and good electrical conductivity, the resulting Pt/N-GNR hybrid possesses superior electrocatalytic ability toward methanol oxidation reaction.